**ORIGINAL ARTICLE**

# Numerical analyses of long fiber–reinforced polymeric sheets processed by Single Point Incremental Forming

Romina Conte[1] · Giuseppe Serratore[1] · Giuseppina Ambrogio[1] · Francesco Gagliardi[1]

**Abstract**

Polymeric matrix composites (PMCs) have gained increasing relevance in different industrial applications and their employment results to be a necessity in the production of lightweight structures. The manufacturing solutions, which allow to properly shape PMC panels, need molds for shaping the material reducing the process flexibility. In this context, the single point incremental forming (SPIF) could be a valuable process solution if properly customized to the PMC properties. Herein, a possible process variant is introduced and its capability in forming long fiber–reinforced thermoplastics was evaluated. To achieve this aim, a numerical model was implemented focusing the attention, first, on the material properties that have to be considered for a proper model construction. The performed numerical simulations showed the applicability of SPIF to shape PMC sheets. Furthermore, the executed simulations pointed out the influences of some variables on the quality of the formed parts showing possible arising of defects, such as wrinkling and rippled surfaces, at different process conditions and providing a first proof of concept of the proposed working solution.

## 1 Introduction

Modern manufacturing systems are characterized by the increasing demand of customized products and, therefore, by the request of flexible processes, which can allow the time to market reduction and a higher customer's satisfaction.

The single point incremental forming (SPIF) is a process in which flexibility has represented its main point of strength, today more than ever due to the current production system, especially when small batches or prototypes have to be produced. The process does not require any dies to impress the desired shape to the sheet, but the controlled movement of a forming tool allows a local, continuous, and plastic deformation of the material [1]. SPIF was first carried out for shaping metal sheets [2], but its application was then extended to other materials, like polymers [3] and composites [4], due to the increasing necessity of a cost-efficient production of high-quality lightweight components. In fact, in some sectors, such as aerospace, automotive, biomedical,

and rapid prototyping, these materials have gained great attention owing to their specific properties.

When polymers have to be processed, heat and pressure are the main parameters to set if conventional techniques are performed (i.e., thermoforming, injection, and blow molding), and mostly, the temperature, since its value influences the material flow (molten or rubbery state), as well as the transition phases and the material degradation. The first reported attempt of forming a polymer by SPIF is attributed to Franzen et al. [5]. The authors performed the process at room temperature on commercial polyvinylchloride (PVC) sheets investigating the main parameters and the formability limits, and geometry accuracy of the shaped conical parts. The mechanisms that cause the failure modes were also identified. Furthermore, forming limit diagrams were built determining the material formability. Finally, the dimensional accuracy of the manufactured parts and the color variation of the processed polymer were evaluated, too [3]. Le et al. [6] and Silva et al. [7] performed SPIF, on polypropylene (PP) and PVC sheets, respectively, aiming to deeply investigate the influence of the main process parameters and their interaction during the forming phase. Marques et al. [8] extended their experimental results on four different thermoplastic polymers evaluating the formability limits,

✉ Romina Conte
romina.conte@unical.it

1   University of Calabria, via P. Bucci Cubo 45C – 87036 Arcavacata di Rende (CS), Rende, Italy

identifying the failure modes, and explaining the stress state, which was mainly related to the tool radius. Davarpanah et al. [9] examined how some process parameters, specifically the step depth and the tool speed, affect the experimental results in terms of failure (tearing and wrinkles), pointing out that the greater the depth is, the greater the formability is. In addition, the monitoring of the forming forces allowed understanding when the transition from tearing to wrinkling occurs. Also, Bagudanch et al. [10] focused the attention on the forces which decrease during the process, when the rotational speed of the tool increases. The authors tried to predict forces by using a model used for metals, but accurate results were not obtained. Finally, Conte et al. [11] and Ambrogio et al. [12] performed hot SPIF processing sheets of different thicknesses made of a polymer characterized by a glass transition temperature above the room temperature. Analyzing what already published, it is possible to state that experimental research was, therefore, performed, mainly.

Concerning the research activities based on finite element (FE) analyses, Sy and Nam [13] examined the deformation of PP sheets by numerical simulations, aiming at predicting the springback and thickness variances. A numerical investigation was carried also out by Medina-Sanchez et al. [14] for predicting axial forces by using a FE method, which considers a hyperelastic-plastic constitutive equation, and a simple semi-analytical model that extends the known specific energy concept used in machining.

Simultaneously, researchers focused their attention also on reinforced polymeric matrices, in other words on polymer matrix composites (PMCs), owing to their great performances and their increasing application in several fields. SPIF, being a versatile and flexible process, well adapts to the downstream workability of composites, even though limited studies have been carried out considering the wide variety of composites and properties to consider. Fiorotto et al. [4] presented a preliminary study on the applicability of SPIF directly to composite materials. The main observed problems were related to the difficulty of deforming plastically the composite and to the removal of the resin from the sheet surface due to the action of the forming tool. Therefore, the authors decided to use diaphragms made of two different materials for improving the formability, for correctly shaping the component, and for avoiding the development of wrinkles. Conte et al. [15] investigated the workability by SPIF of polyamide-6 (PA 6) reinforced with short glass fibers. The process was carried out using an aluminum dummy sheet, which is in direct contact with the forming tool, and acts as a support to facilitate the composite shaping without ruining its surface. Furthermore, considering the preliminary studies carried out by the authors [16], a heating source was included in the equipment to allow the material deformation guaranteeing the process temperature monitoring. Material formability, thickness distribution, and part accuracy were

analyzed, and the influence of the main process parameters, such as wall angle, step depth, and process temperature, was examined [17]. Davarpanah and Malhotra [18] focused on the feasibility of forming polymer-metal laminates by SPIF. Experiments allowed them to observe three failure modes, such as delamination, tearing, and polymeric surface galling. Al-Obaidi et al. [19] applied an innovative method based on SPIF assisted by a hot air heating for producing medical implants made of glass fiber–reinforced polymers (GFRPs). Specifically, the glass fibers were placed between two Teflon layers and protected with two dummy metal sheets from the tool and from the heating generated by friction. The authors observed and analyzed cracks and voids and aimed at demonstrating that the matrix melting could be reduced, as well as the distortion of the final cone-shaped part. Torres et al. [20] experimented the formability of a composite material made of a biodegradable thermoplastic matrix reinforced with short natural fibers introducing a heated fluid to facilitate the formability. Recently, Xiao et al. [21] developed a hybrid technique based on SPIF for shaping carbon fiber–reinforced plastics (CFRP). A mild steel layer was applied over the CFRP acting as a dummy sheet for supporting the deformation of the underlying composite. Furthermore, a FE model based on mesoscale dimensions was built and the results compared with the experiments, demonstrating that the simulation can accurately predict the deformation.

The study of the scientific literature highlighted a lack of knowledge on the numerical analysis of SPIF when composites are processed and, furthermore, the research was performed mainly on polymeric matrices reinforced by short fibers. The authors aimed at filling up this gap by formulating a numerical model, which can be useful in the analysis of SPIF on PMC, if long fibers are utilized as reinforcement in a thermoplastic resin. Specifically, once defined the model and discussed its characteristics, the feasibility of SPIF on long fiber–reinforced thermoplastics was analyzed, numerically. The model was built considering the experimental idea proposed by [20], who included a fluid in the working zone for a uniform distribution of the heat on the processed material. Moreover, the authors of this work took also into account the equipment's scheme they presented in [22]. Herein, the pressure of a fluid was controlled inside a hermetic chamber employing an expansion tank and relief valves to allow PMC and dummy sheet to be in contact during the forming phase. It is worth pointing out the importance and the role attributed to the dummy sheet for the process dynamics, in addition to what first highlighted by Fiorotto et al. [4], since this metallic diaphragm permits the composite blank to be not clamped to the SPIF frame, allowing its formability despite this is reinforced by long fibers. The proposed idea does not affect the process flexibility that is the main advantage of SPIF, if this process is compared to the traditional stamping of sheet. Indeed, the higher process costs, related to the equipment's components

and to the wasted metallic sheet, can be justified considering that components made of long fiber–reinforced composites are produced.

## 2　Numerical model

### 2.1　Material implementation and configuration of the PMC sheets

The FE model was developed starting from a proper material model to be implemented for the definition of the virtual composite sheet. This sheet is made of GFRP. The PP, whose forming temperature is around 220 °C, was chosen as the matrix, considering its hygroscopic characteristics for a next experimental validation of the proposed process configuration. Long E-glass fibers, not stitched in the prepreg laminas, are the type of reinforcement. The volume fraction of the fibers in each lamina is 60%. The virtual composite sheet was built considering an overlapping of laminas, moving from unidirectional to quasi-isotropic conditions. The investigated configurations are described in Table 1.

The mechanical properties of the lamina at the working temperature are reported in Table 2.

Laminas are set considering their linear elastic properties and implementing the Hashin's damage model [24] to study the matrix and\or fiber failures. This is a quadratic stress-based failure model able to predict four different damage initiation mechanisms, which involve fiber tension, fiber compression, matrix tension, and matrix compression by means of four different quadratic relations [25]:

Fiber tensile damage $(\hat{\sigma}_{11} \geq 0)$: $F_f^t = \left(\frac{\hat{\sigma}_{11}}{X_T}\right)^2 + \left(\frac{\hat{\tau}_{12}}{S_L}\right)^2$

$$(1)$$

Fiber compressive damage $(\hat{\sigma}_{11} < 0)$: $F_f^c = \left(\frac{\hat{\sigma}_{11}}{X_C}\right)^2$ $\quad(2)$

Matrix tensile damage $(\hat{\sigma}_{22} \geq 0)$: $F_m^t = \left(\frac{\hat{\sigma}_{22}}{Y_T}\right)^2 + \left(\frac{\hat{\tau}_{12}}{S_L}\right)^2$

$$(3)$$

Matrix compressive damage $(\hat{\sigma}_{22} < 0)$: $F_m^c = \left(\frac{\hat{\sigma}_{22}}{2S_T}\right)^2 + \left[\left(\frac{Y^C}{2S_T}\right)^2 - 1\right]\frac{\hat{\sigma}_{22}}{Y_C} + \left(\frac{\hat{\tau}_{12}}{S_L}\right)^2$

$$(4)$$

**Table 2** Mechanical properties of the utilized prepreg [23]

| Parameters 220 °C | E11 | E22 | µ12 | G12 | G23 |
|---|---|---|---|---|---|
| Value | 2.5 GPa | 0.5 MPa | 0.35 | 0.2 MPa | 0.2 MPa |

where $\hat{\sigma}_{11}$, $\hat{\sigma}_{22}$, and $\hat{\tau}_{12}$ are components of the effective stress tensor $[\hat{\sigma}]$, while $X_T$, $X_C$, $Y_T$, $Y_C$, $S_L$, and $S_T$ denote the longitudinal tensile strength, the longitudinal compressive strength, the transverse tensile strength, the transverse compressive strength, the longitudinal shear strength, and the transverse shear strength respectively. When one of these relations meets a value of 1.0, or higher, the respective failure mode occurs. The Hashin's damage evolution was defined by setting the fiber tensile/compressive fracture energy and the matrix tensile/compressive fracture energy to capture the behavior of the material after one or more damage initiation criteria [26]. The parameters of the constitutive damage model of the lamina were set according to [27]. However, since these parameters are available at room temperature, and considering that the virtual working temperature is 220 °C, the Saafi's model [28] was implemented to scale them, proportionally, considering the reduction factors $k_f$ and $k_E$, respectively, for the strength properties and for the elastic moduli:

$$k_f = 1 - 0.025T \ for \ 0 \ °C < T < 400 \ °C \quad (5)$$

$$k_E = \begin{cases} 1 & for & 0 \leq T \leq 100 \ °C \\ 1.25 - 0.0025T & for & 100 \leq T \leq 300 \ °C \\ 2 - 0.005T & for & 300 \leq T \leq 400 \ °C \end{cases} \quad (6)$$

By doing so, the damage initialization and evolution were also considered in the analysis. The dummy sheet employed as a cover is a 2-mm-thick aluminum alloy (AA-6056). The plasticity behavior of the AA-6056 sheet was modelled according to the Johnson-Cook formulation:

$$\sigma = (A + B\varepsilon_p^{\ n})\left(1 + Cln\frac{\dot{\varepsilon}}{\dot{\varepsilon}_0}\right)(1 - T^m) \quad (7)$$

with the material parameters, reported in Table 3, that were taken from [29].

**Table 1** Configuration of GFRP panels

| Laminate sequences | Diameter (mm) | Lamina thickness (mm) | Laminate thickness (mm) |
|---|---|---|---|
| [0/0/0/0]$_s$ | 160 | 0.25 | 2 |
| [0/45/-45/90]$_s$ | 160 | 0.25 | 2 |
| [0/90/0/90]$_s$ | 160 | 0.25 | 2 |

**Table 3** Johnson-Cook parameters for the AA-6056 [29]

| $A$ (MPa) | $B$ (MPa) | $n$ | $C$ | $m$ | $T_{melt}$ (°C) |
|---|---|---|---|---|---|
| 335 | 158 | 0.2143 | 0.0275 | 0.377 | 580 |

**Fig. 1** Cross-section view of the FE model
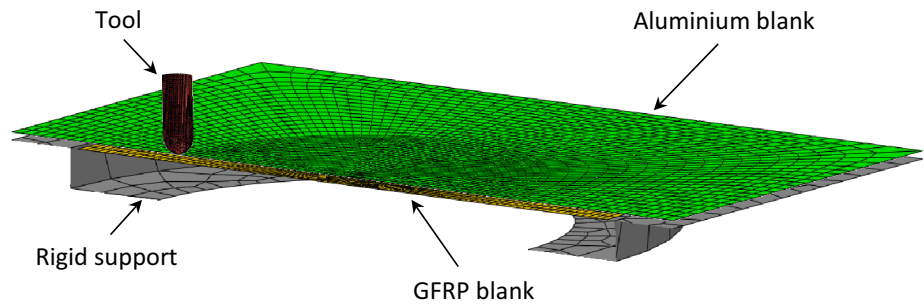
## 2.2 Numerical model of the process

The finite element model of the proposed SPIF process was performed by the FE commercial code Abaqus/CAE. Figure 1 shows the assembly cross-section of the FE model based on the process strategy previously described.

In detail, the rotating forming tool, modelled as a rigid body, is in contact with a squared aluminum blank characterized by a 200 mm side and fixed in the periphery on a steel frame modelled as a rigid body. A Coulomb's friction coefficient of 0.1 was considered between the tool and the metallic sheet [30]. The outer edge of the GFRP panel beneath the metallic blanks is fixed along the vertical direction and subjected to the hydrostatic pressure simulating the presence of a pressurized fluid. A constant pressure was applied under the GFRP plate, as shown in Fig. 2. A frictionless approach was used between the two sheets, which were modelled as deformable bodies using shell elements (S4R). The Simpson's integration rule with 5 integration points was modelled along the thickness direction, and about 5000 elements for the aluminum diaphragm and 6500 elements for the GFRP sheet were employed. An explicit solver with time and mass scaling was utilized to speed up the simulation time. Specifically, a semi-automatic mass scaling was implemented with a target time increment equal to 2e-6 s. The toolpath was defined by three tabular amplitudes while the total simulation time was imposed equal to 6 s.

## 2.3 Investigated process variables

A truncated cone was numerically formed. The cone is characterized by a slope angle of 30°, a final height of 25 mm, and a base diameter of 100 mm. The effects on the quality of the formed parts, focusing the attention on surface quality, shape accuracy, and/or local thinning of the sheet, were evaluated by changing the following:

1. The configurations of the GFRP panels as previously reported in Table 1.
2. The value of the pressure on the back face of the GFRP panels. Constant values from 0.01 to 0.2 MPa during the whole forming phase were evaluated.
3. The initial shape of the GFRP panels to be formed.
4. The path direction of the forming tool. Specifically, the strategy by using clockwise and counterclockwise movement of the forming tool between two subsequent coils for the entire trajectory path was compared to the traditional strategy, which is characterized by the same direction of the tool movement for the whole process.

## 3 Results of the FE simulations

This section deals with the analysis of the numerical results obtained by the performed simulations on the described SPIF process. Specifically, the three different configurations
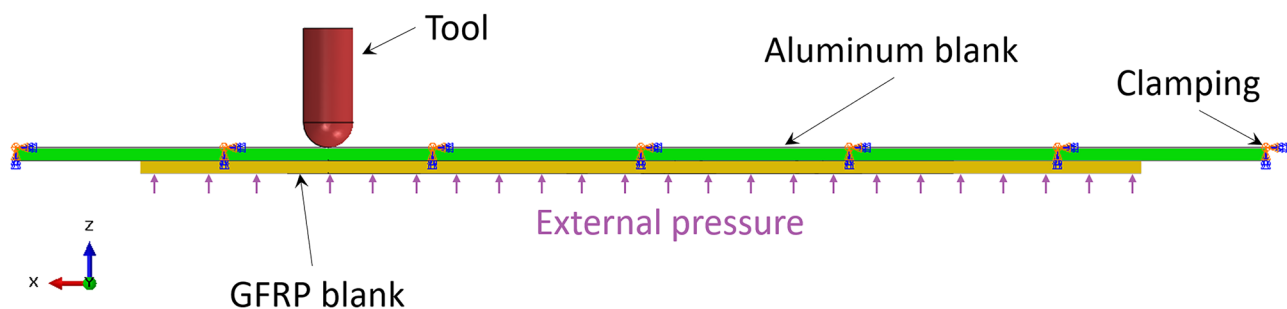


**Fig. 2** Boundary conditions and loads of the FE model

of the GFRP panels were evaluated in terms of formability, thickness distribution, and shape accuracy. Subsequently, the influences of back pressure in terms of magnitude and application methodology, initial shape of the panels to be formed, and tool's movement direction were investigated on the most challenging configuration that, considering the formability defects, was the quasi-isotropic conditions of the panel.

## 3.1 Analysis on the sheet configurations

Figure 3a reports the back side of the GFRP sheets for the three investigated configurations. These analyses were performed setting a low back pressure of 0.01 MPa. The traced circumference represents the ideal shape of a section of the truncated cone if a homogeneous sheet movement is
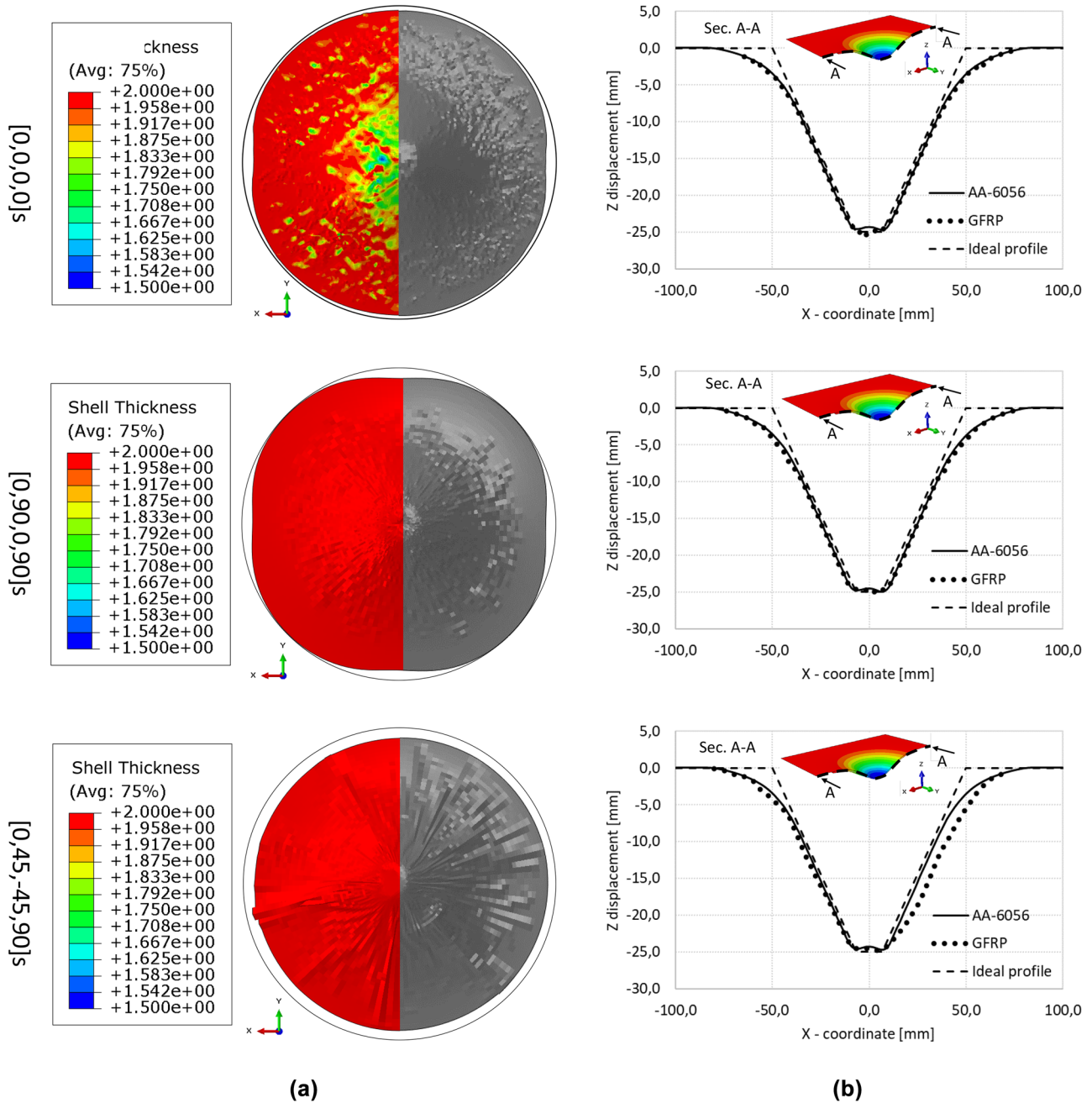


**Fig. 3** Comparison of **a** thickness distribution and **b** shape accuracy for an imposed back pressure of 0.01 MPa for the three panel configurations

achieved during the forming phase. Representations of the surface quality and of the thickness distribution for each configuration were also illustrated. The influence of the different properties of the formed sheets is evident considering the shape, the surface, and the thinning of the conical part. Specifically, starting from the unidirectional configuration [0,0,0,0]$_s$, the anisotropic properties of the sheet result in a non-homogeneous sheet movement. Indeed, the long fibers, aligned along the x-axis, provide higher strength to the sheet along this direction. This results in a more relevant sheet movement along the y-axis obtaining an elliptical shape of the formed section. The thinning of the sheet for this configuration results to be restrained along the side of the truncated conical shape and slightly notable just on its top, where a maximum true strain of around 0.15 (absolute value) was observed. Concerning the sheet movement, the same behavior can be observed for the configuration [0,90,0,90]$_s$. But, in this case, the sheet's diagonal lines are the weakest directions toward which the material moves more. The outcome is a rounded squared section. The quasi-isotropic configuration, i.e., [0,45,-45,90]$_s$, is, instead, characterized by an uniform deformation along the main directions preserving the circular shape of the section as the imposed tool trajectory. For these last two configurations, the panel was shaped without affecting the initial thickness of the sheet (Fig. 3a). Regarding the surface defects, for the quasi-isotropic configuration, the arising of wrinkling appears along the conical side with an out-of-plane deformation that has to be taken into account. This phenomenon, instead, was not observed for the first two configurations, where preferential directions of the material movement on the sheet plane prevent the out-of-plane repositioning. For these first two cases, the non-homogeneous deformations result in a surface rippling, which is a less evident phenomenon (Fig. 3a). Finally, looking at the obtained formability for each configuration, this outcome was evaluated observing the GFRP sheet adhesion to the dummy aluminum side. In Fig. 3b, the cross-section profiles, extracted from the composite and metallic sheet, were overlapped, removing their thickness presence for the whole investigated configurations. These profiles were related to the ideal profile of the truncated cone, which is considered reference in relation to the imposed tool path. A consistent superimposition for each configuration was observed resulting in the conclusion that the low back pressure, i.e., 0.01 MPa, provides a proper support to allow the adhesion of the composite to the metal. This can be justified considering the very low mechanical GFRP properties at the imposed working temperature, as previously reported in Table 2.

## 3.2 Analysis on the effect of the back pressure

The hydrostatic pressure on the back side of the GFRP was increased to verify if its value could affect the defects

**Fig. 4** Comparison of **a** the rippled surfaces and thickness distribution and **b** the achieved shapes of the formed parts for an imposed back pressure of 0.01, 0.05, 0.10, and 0.20 MPa for the configuration [0,90,0,90]$_s$

highlighted in the previous section, i.e., rippled surfaces and wrinkling depending on the investigated cases. The maximum value of the pressure that can be set depends on the strength of the metallic sheet, whose nominal shape, function of the imposed tool trajectory, does not have to be affected by the back pressure. Four different levels of internal pressure were considered, i.e., 0.01, 0.05, 0.10, and 0.20 MPa, starting from the analysis of the rippled surfaces observed for the configurations [0,0,0,0]$_s$ and [0,90,0,90]$_s$. This phenomenon was reduced significantly just passing from 0.01 to 0.05 MPa, as observable in Fig. 4a, where the panel configuration [0,90,0,90]$_s$ was displayed as reference. This result shows the healthy impact of the increment of the back pressure for the softening of this defect. However, investigating the higher-pressure levels, i.e., 0.10 and 0.20 MPa, a process limitation was observed (Fig. 4a). Indeed, at these pressure values, the imposed force on the bottom side of the sheets overcomes the strength of the metallic dummy sheets and, consequently, the inaccuracies on the final product shapes, if these are compared to the ideal profile, increase (Fig. 4b).

The wrinkling defects, instead, appeared more complicated to be solved by just increasing the back pressure, as depicted in Fig. 5a. Indeed, the numerical evidence shows that the increment of the pressure results in the formation of a reduced number of wrinkles on the conical surface, but these defects are more evident and relevant. In other words, a higher hydrostatic pressure on the backside of the quasi-isotropic GFRP sheet focused the out-of-plane material movement in localized areas, where the material in excess is accumulated. Once the wrinkles arise, just the increment of the pressure cannot solve the problem as numerically proved arriving to set a pressure of 0.2 MPa, which is the maximum one tested. Furthermore, at this value, the obtainable shape of the metallic sheet results to be affected, significantly, with respect to the ideal profile, owing to the sheet movement along the z direction for the elevated back pressure, as highlighted in Fig. 5b.

According to the reported numerical evidences, the discussed SPIF strategy allows achieving sound truncated cones easier if some directions on the plane of the long fiber–reinforced polymeric sheets are characterized by reduced strength to permit a non-homogeneous material deformation. In other words, this means that not quasi-isotropic sheets are more suitable to be formed by the proposed strategy.
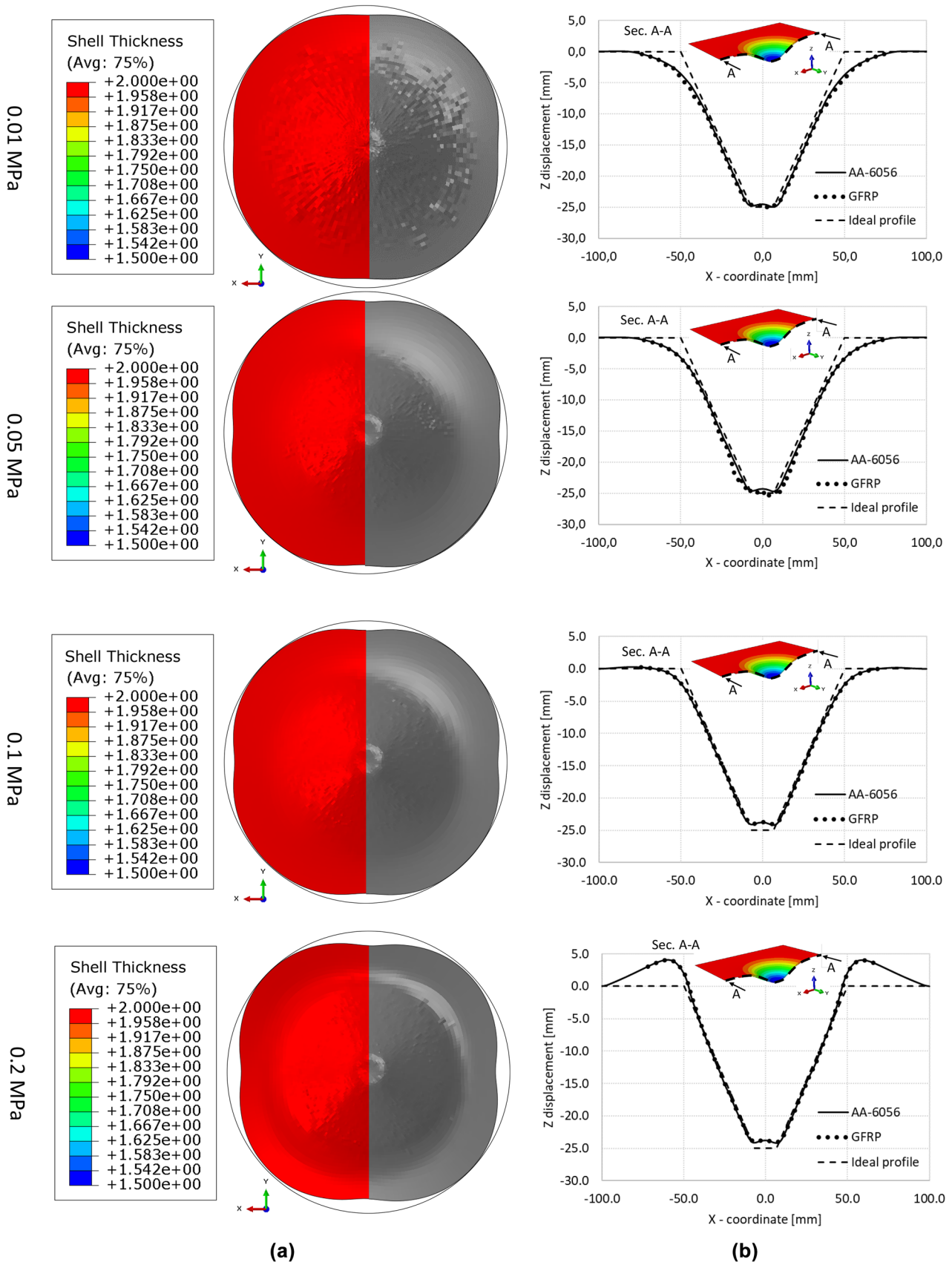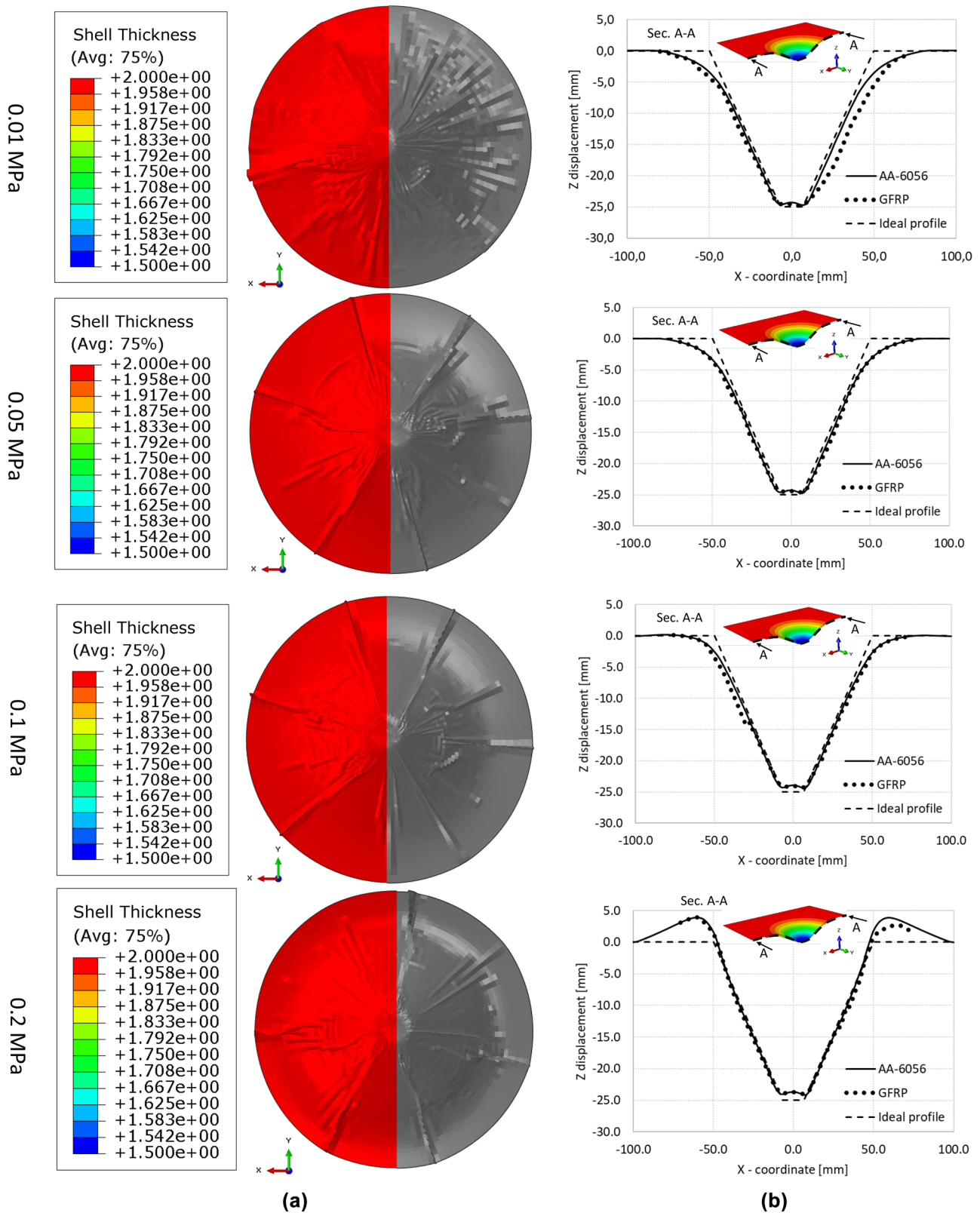
**Fig. 5** Comparison of **a** the wrinkled surfaces and thickness distribution and **b** the achieved shape of the formed parts for an imposed back pressure of 0.01, 0.05, 0.1, and 0.2 MPa for the configuration [0,45,-45,90]$_s$
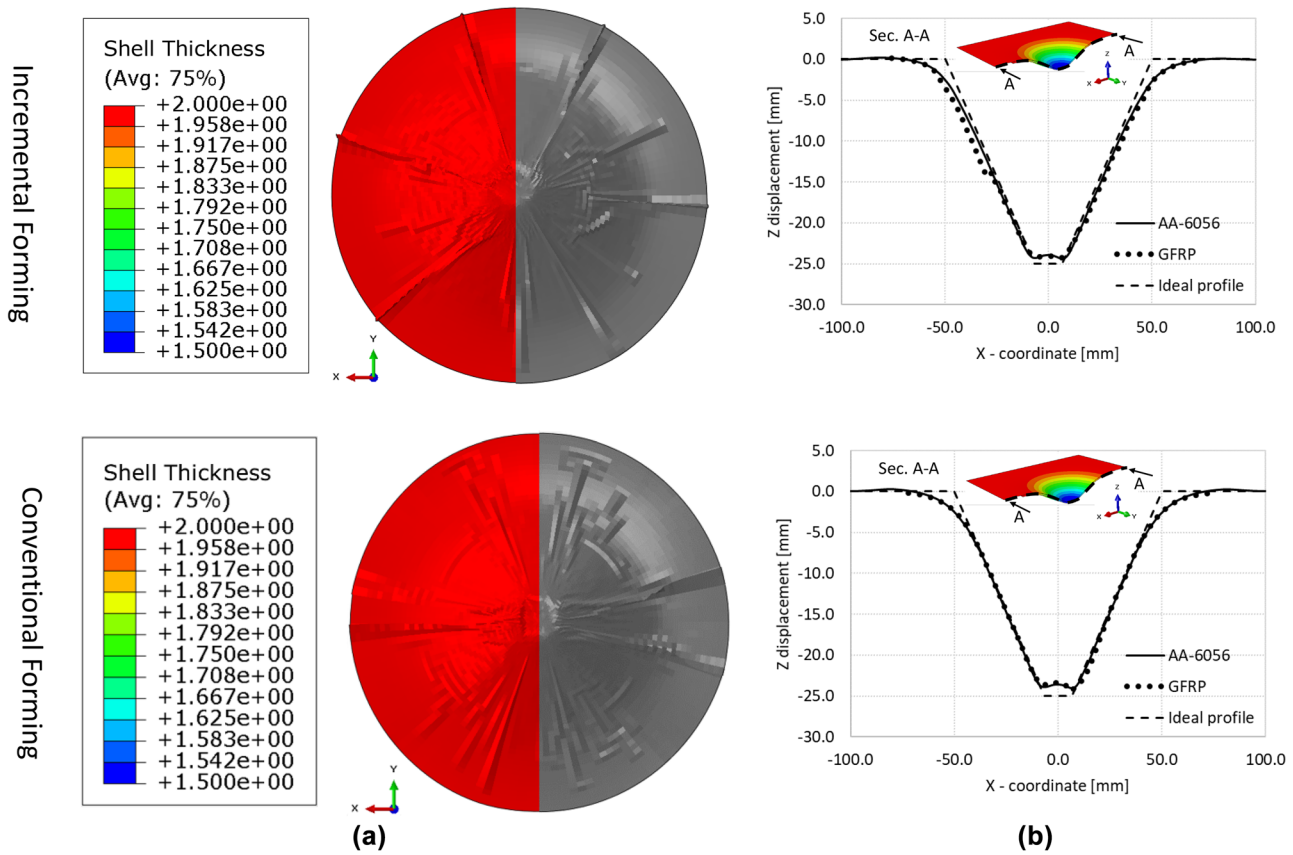
**Fig. 6** Comparison of **a** the wrinkled surfaces and thickness distribution and **b** the achieved shape of a composite panel incrementally or conventionally formed by a constant pressure of 0.1 MPa for the configuration [0,45,-45,90]$_s$

### 3.3 Wrinkling development owing to specific process conditions for the [0,45,-45,90]$_s$ panel

The wrinkling phenomenon for the quasi-isotropic sheet was further numerically investigated. First of all, a conventional pressure forming sequence for composite materials was analyzed shaping the panel by an imposed constant pressure of 0.1 MPa on an already formed mold (Fig. 6).

This analysis showed that the out-of-plane material movement is a process characteristic that takes place even
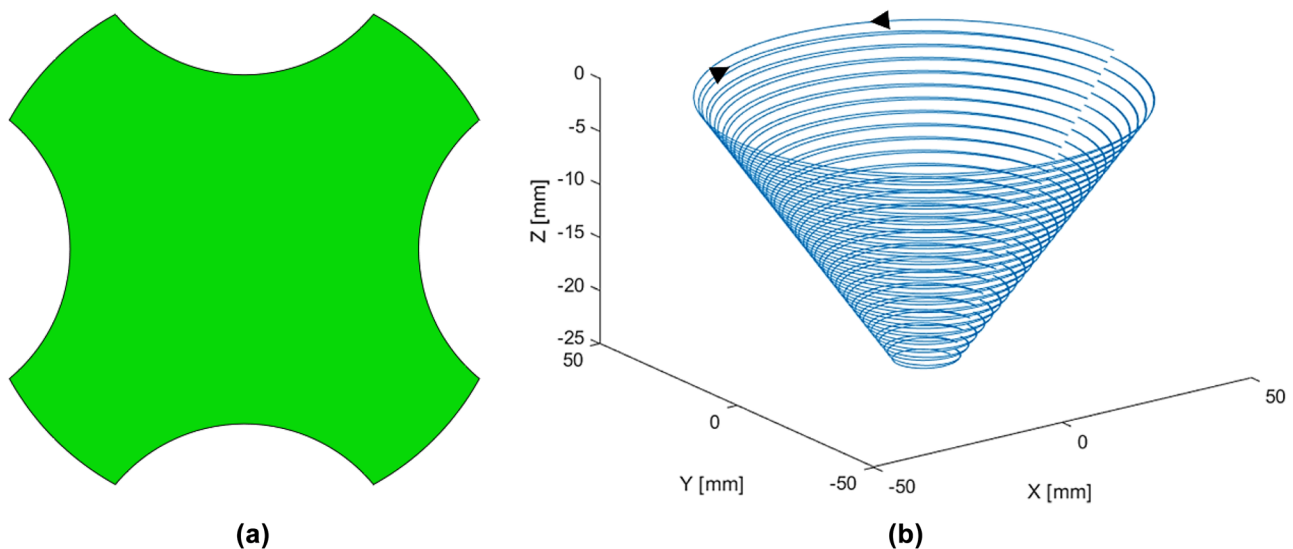


**Fig. 7** **a** Initial shape of the sheared GFRP sheet and **b** the imposed clockwise and counterclockwise path

for the conventional forming of quasi-isotropic composite panels, even if wrinkles are less evident and assembled. The incremental forming strategy, therefore, affects somehow the wrinkling phenomenon. For this reason, process changes were introduced to modify the history of the incremental deformation aiming at an attenuation of the material out-of-plane movements. Two different approaches were analyzed. Specifically, first, the sheet to be formed was sheared to reduce its strength in specific directions. The horizontal and the vertical directions were chosen to test the influence of this solution (Fig. 7a). In a second strategy, the movement of the forming tool was changed from clockwise to counterclockwise and vice versa passing from one coil to the next one for the entire incremental

forming path (Fig. 7b). This change was proposed because it affects the stress distribution inside the formed sheet compared to the constant tool direction for the whole process as already proved in processing polymeric sheets by SPIF, where the clockwise and counterclockwise coil path was employed to reduce twisting of the formed parts [31].

The backsides of the composite sheets incrementally formed with a constant hydrostatic pressure of 0.1 MPa and by using the discussed process changes were reported in Fig. 8, where the comparison with the first virtual processed part using the standard conditions and the same pressure was provided as reference.

The modification of the initial shape of the sheet resulted in an alteration of the wrinkles considering both
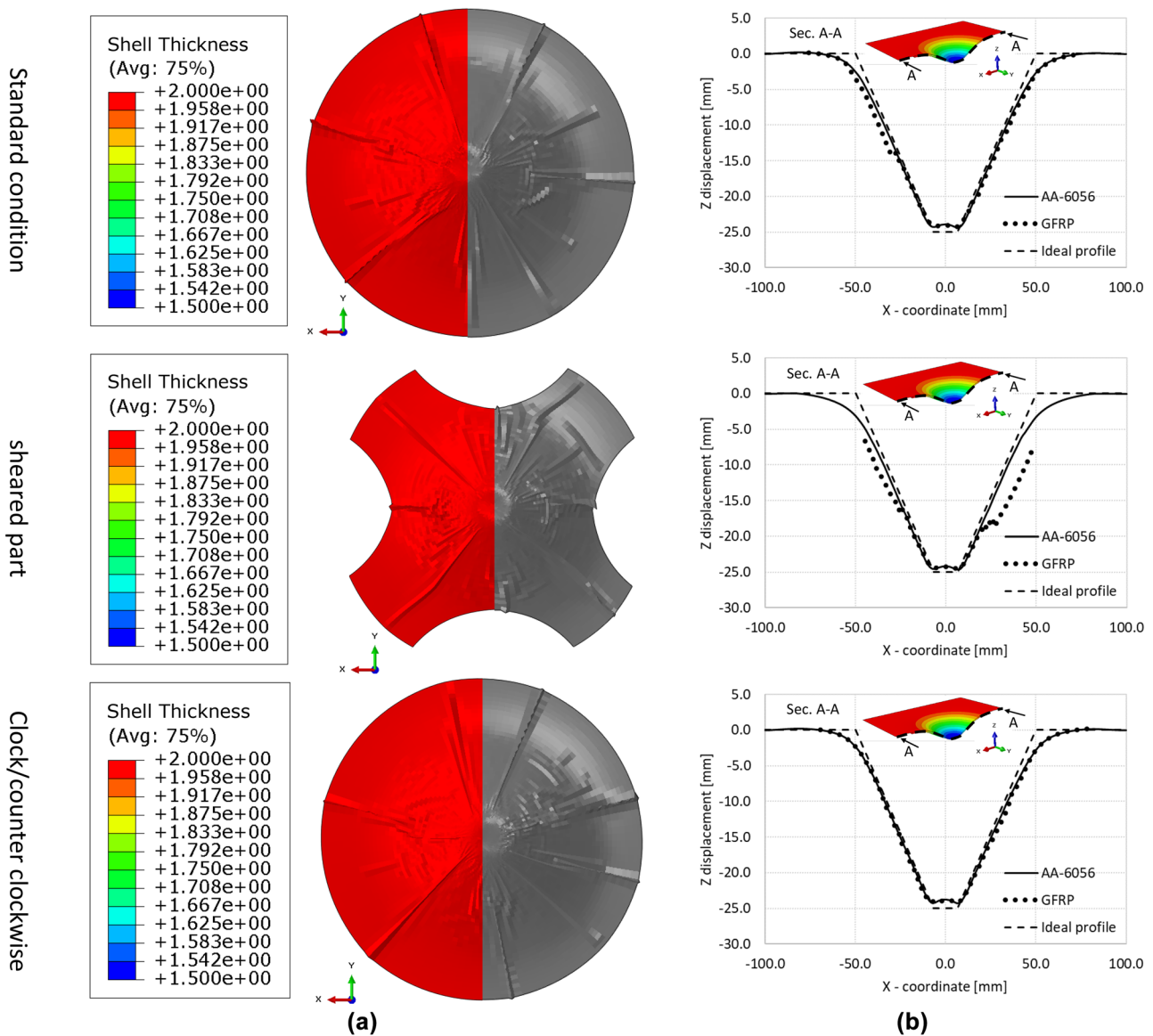


**Fig. 8** **a** Wrinkling development and **b** shape accuracy of the quasi-isotropic configuration [0,45,-45,90]$_s$ using (1) standard process conditions, (2) a sheared panel, and (3) clockwise and counterclockwise tool paths for a constant hydrostatic pressure of 0.1 MPa

number and dimensions, while the change in the forming tool direction seems not affecting this phenomenon. Nevertheless, the reported variables deserve accurate studies in a perspective of the SPIF optimization for its employment in forming long fiber–reinforced polymers.

## 4 Conclusion

The feasibility of employing SPIF to process long fiber–reinforced polymeric sheets was evaluated by a numerical model based on specific process characteristics, considering that long fibers cannot be stretched during the forming phase due to their brittle behavior. A material model was implemented to be able to consider matrix and\or fiber failures at the imposed working temperatures. The developed numerical tool was employed to test some variables, which could affect the process dynamics considering both a typical composite material peculiarity, i.e., the laminas configuration, moving from unidirectional to quasi-isotropic conditions, and process conditions, i.e., the value of the back pressure, the direction of the forming tool, and the initial shape of the formed sheet.

Back pressure, around 0.01 MPa, guaranteed the adhesion of the composite to the dummy metallic sheet following the nominal shape and guaranteeing the components' shape accuracy obtainable by the process. Furthermore, the thickness distributions of the truncated cones resulted to be not affected by the SPIF being the composite blank not clamped and shapable without its stretching. Typical defects arising during the forming of composite laminates were, instead, observed, such as wrinkling and not uniform deformation of the sheets. Specifically, the arising of wrinkling, ascribable to an out-of-plane sheet deformation, was observed for the quasi-isotropic condition for which the material repositioning cannot exploit preferential movement directions. Moving to the non-isotropic sheets, surface rippling was instead detected. Increasing the hydrostatic pressure on the back side of the GFRP, up to the maximum allowable values related to the strength of the metallic dummy sheet, for restriction due to the obtainable accuracy of the product's shape, permitted rippling defects to be mitigated while it affects slightly the out-of-plane material movements. Therefore, the numerical analyses evidenced how SPIF strategy allows achieving sound shapes easier if some directions on the plane of the long fiber–reinforced polymeric sheets are characterized by reduced strength to allow a non-homogeneous material deformation.

The wrinkling evolutions was investigated to specific working conditions, such as initial shape of the composite sheet to be formed and direction of the formed tool's path showing the potentiality of the proposed numerical model, which needs to be experimentally validated before being used in the optimization phase of this process, that could result to be an effective flexible process solution to process long fiber–reinforced polymers.

## Declarations

**Competing interests** The authors declare no competing interests.

**Disclosure** The submission of the authors' paper implies that it has not been previously published, that it is not under consideration for publication elsewhere, and that it will not be published elsewhere in the same form without the written permission of the editors.

## References

1. Martins PAF, Bay N, Skjoedt M, Silva MB (2008) Theory of single point incremental forming. CIRP Ann 57:247–252. https://doi.org/10.1016/j.cirp.2008.03.047
2. Fratini L, Ambrogio G, Di Lorenzo R et al (2004) Influence of mechanical properties of the sheet material on formability in single point incremental forming. CIRP Ann 53:207–210. https://doi.org/10.1016/S0007-8506(07)60680-5
3. Martins PAF, Kwiatkowski L, Franzen V et al (2009) Single point incremental forming of polymers. CIRP Ann 58:229–232. https://doi.org/10.1016/j.cirp.2009.03.095
4. Fiorotto M, Sorgente M, Lucchetta G (2010) Preliminary studies on single point incremental forming for composite materials. Int J Mater Form 3:951–954. https://doi.org/10.1007/s12289-010-0926-6
5. Franzen V, Kwiatkowski L, Martins PAF et al (2009) Single point incremental forming of PVC. J Mater Process Technol 209:462–469. https://doi.org/10.1016/j.jmatprotec.2008.02.013
6. Le VS, Ghiotti A, Lucchetta G (2008) Preliminary studies on single point incremental forming for thermoplastic materials. Int J Mater Form 1:1179–1182. https://doi.org/10.1007/s12289-008-0191-0

7. Silva MB, Alves LM, Martins PAF (2010) Single point incremental forming of PVC: experimental findings and theoretical interpretation. Eur J Mech A/Solids 29:557–566. https://doi.org/10.1016/j.euromechsol.2010.03.008

8. Marques TA, Silva MB, Martins PAF (2012) On the potential of single point incremental forming of sheet polymer parts. Int J Adv Manuf Technol 60:75–86. https://doi.org/10.1007/s00170-011-3585-y

9. Davarpanah MA, Mirkouei A, Yu X et al (2015) Effects of incremental depth and tool rotation on failure modes and microstructural properties in single point incremental forming of polymers. J Mater Process Technol 222:287–300. https://doi.org/10.1016/j.jmatprotec.2015.03.014

10. Bagudanch I, Garcia-Romeu ML, Centeno G et al (2015) Forming force and temperature effects on single point incremental forming of polyvinylchloride. J Mater Process Technol 219:221–229. https://doi.org/10.1016/j.jmatprotec.2014.12.004

11. Conte R, Gagliardi F, Ambrogio G et al (2017) Performance analysis of the incremental sheet forming on PMMA using a combined chemical and mechanical approach. AIP Conf Proc 1896:080026

12. Ambrogio G, Gagliardi F, Conte R, Russo P (2019) Feasibility analysis of hot incremental sheet forming process on thermoplastics. Int J Adv Manuf Technol 102:937–947. https://doi.org/10.1007/s00170-018-3180-6

13. Sy LV, Nam NT (2012) A numerical simulation of incremental forming process for polymer sheets. Int J Model Simul 32:265–272. https://doi.org/10.2316/Journal.205.2012.4.205-5752

14. Medina-Sanchez G, Garcia-Collado A, Carou D, Dorado-Vicente R (2018) Force prediction for incremental forming of polymer sheets. Materials 11:1597. https://doi.org/10.3390/ma11091597

15. Conte R, Ambrogio G, Pulice D et al (2017) Incremental sheet forming of a composite made of thermoplastic matrix and glass-fiber reinforcement. Procedia Eng 207:819–824. https://doi.org/10.1016/j.proeng.2017.10.835

16. Conte R, Ambrogio G, Gagliardi F et al (2017) Preliminary experimental analysis on incremental forming of fiberglass reinforced polyamide 6. AITeM 2017

17. Ambrogio G, Conte R, Gagliardi F et al (2018) A new approach for forming polymeric composite structures. Compos Struct 204:445–453. https://doi.org/10.1016/j.compstruct.2018.07.106

18. Davarpanah MA, Malhotra R (2018) Formability and failure modes in single point incremental forming of metal-polymer laminates. Procedia Manuf 26:343–348. https://doi.org/10.1016/j.promfg.2018.07.042

19. Al-Obaidi A, Kunke A, Kräusel V (2019) Hot single-point incremental forming of glass-fiber-reinforced polymer (PA6GF47) supported by hot air. J Manuf Process 43:17–25. https://doi.org/10.1016/j.jmapro.2019.04.036

20. Torres S, Ortega R, Acosta P, Calderón E (2021) Hot incremental forming of biocomposites developed from linen fibres and a thermoplastic matrix. Strojniški Vestn J Mech Eng 67:123–132. https://doi.org/10.5545/sv-jme.2020.6936

21. Xiao X, Kim J-J, Oh S-H, Kim Y-S (2021) Study on the incremental sheet forming of CFRP sheet. Compos A Appl Sci Manuf 141:106209. https://doi.org/10.1016/j.compositesa.2020.106209

22. Gagliardi F, Conte R, Serratore G et al (2022) SPIF performed by a controlled temperature room for polymer-based materials. XV Convegno dell'Associazione Italiana delle Tecnologie Manifatturiere

23. Liu K, Zhang B, Xu X et al (2019) Simulation and analysis of process-induced distortions in hemispherical thermostamping for unidirectional thermoplastic composites. Polym Compos 40:1786–1800. https://doi.org/10.1002/pc.24936

24. Hashin Z (1980) Failure criteria for unidirectional fiber composites. J Appl Mech 47:329–334. https://doi.org/10.1115/1.3153664

25. Damage initiation for fiber-reinforced composites. https://abaqus-docs.mit.edu/2017/English/SIMACAEMATRefMap/simamat-c-damageinitfibercomposite.htm?msclkid=ae444b85cf7f11ecac1e598e27f4f04d

26. Damage evolution. https://abaqus-docs.mit.edu/2017/English/SIMACAECAERefMap/simacae-t-prpmechanicaldamageevolution.htm

27. Rahimian Koloor S, Karimzadeh A, Yidris N (2020) An energy-based concept for yielding of multidirectional FRP composite structures using a mesoscale lamina damage model. Polymers 12:157. https://doi.org/10.3390/polym12010157

28. Saafi M (2002) Effect of fire on FRP reinforced concrete members. Compos Struct 58:11–20. https://doi.org/10.1016/S0263-8223(02)00045-4

29. Vivas M, Lours P, Levaillant C, Couret A, Casanove MJ, Coujou A (1996) Some aspects of precipitation hardening in aluminum alloy 6056 T6 – T.E.M. Experiments. Mat Sci Forum 217:1305–1310. https://doi.org/10.4028/www.scientific.net/MSF.217-222.1305

30. Tayebi P, Fazli A, Asadi P, Soltanpour M (2019) Formability analysis of dissimilar friction stir welded AA 6061 and AA 5083 blanks by SPIF process. CIRP J Manuf Sci Technol 25:50–68. https://doi.org/10.1016/j.cirpj.2019.02.002

31. Yang Z, Chen F (2020) Mechanism of twist in incremental sheet forming of thermoplastic polymer. Mater Des 195:108997. https://doi.org/10.1016/j.matdes.2020.108997